Green Synthesis of Manganese-Enriched Zinc Oxide Nanoparticles via Dragon Fruit Peel Extracts and their Photocatalytic activity on Methyl Orange

Kistan A.[1*], Kanchana V.[2], Mohan S.[3] and Chitra M.[4]
1. Department of Chemistry, Panimalar Engineering College, Chennai-600123, Tamil Nadu, INDIA
2. Department of Chemistry, Sree Sastha Institute of Engineering and Technology, Chennai-600123, Tamil Nadu, INDIA
3. Department of Chemistry, Rajalakshmi Engineering College, Chennai-602105, Tamil Nadu, INDIA
4. Department of Chemistry, Chellammal Women's College, Chennai-600032, Tamil Nadu, INDIA
*vishmikrish@gmail.com

Abstract
Methylene orange (MO) is organic dye, unsafe and persevering in the climate. This study was chosen to assess photocatalytic expulsion of MO color from fluid arrangement utilizing Mn doped ZnO nanoparticles. Characterisation of Mn doped ZnO nano particle was performed utilizing Fourier transform infrared spectroscopy (FTIR), Electronic microscopy and X-beam diffraction (XRD). A 5-level-5-factor focal composite plan (CCD) approach-based reaction surface system (RSM) analysis was utilized to indicate the impact of primary cycle factors.

The removal efficiency of dye was acquired more than 90 % in ideal circumstances (10 mg/L, pH: 9, contact time: 91.25 min, Mn-ZnO NP's measurement: 0.77 g/L). Exploratory information was well fitted to pseudo-second request dynamic model (R_2 = 0.989). Therefore, Mn-ZnO NP's can be applicable for treating contemporary wastewater having colour.

Keywords: Mn doped ZnO NP's, Dragon fruit peel extracts, Methyl orange, Degradation efficiency.

Introduction

Researchers from all over the world are particularly interested in the green synthesis of nanoscale materials. We outline a straightforward, reliable, reasonably priced and ecologically friendly method for creating gold, silver and iron nanoparticles making use of a number of biomolecules and phytochemicals as possible stabilisers and reducers. Utilising plant extracts forms the foundation of the environmentally friendly method for the controlled synthesis of nanoparticles with various morphologies[23,36]. Greenly produced nanoparticles can be employed as adsorbents, catalysts, photocatalysts, or alternative agents to remove different organic dyes. The use of biochemically functionalized nanoparticles in engineering may benefit greatly from the kinetic improvement of nanoparticles for the degradation/removal of dyes.

In this study, morphology dependent nanoparticles for the degradation of organic contaminants in wastewater are discussed along with recent plant-mediated methods for producing gold, silver and iron nanoparticles. Overall, the strategy outlined in the study promotes environmental safety and offers a promising substitute for conventional synthesis methods[17,21].

The dragon fruit, also known as *Hylocereus undatus*, contains antioxidants such as flavonoids, phenolic acid and betacyanin. These organic compounds shield cells from the harm. One of the tropical fruits that belongs to the Cactaceae cactus family is the dragon fruit, sometimes referred to as pitaya[9,12,18]. Three primary species of dragon fruit. *Hylocereus undatus* (white flesh with pink skin), *Hylocereus polyrhizus* (red meat with pink skin) and *Selenicereus megalanthus* (white flesh with yellow skin) are available for commercial cultivation.

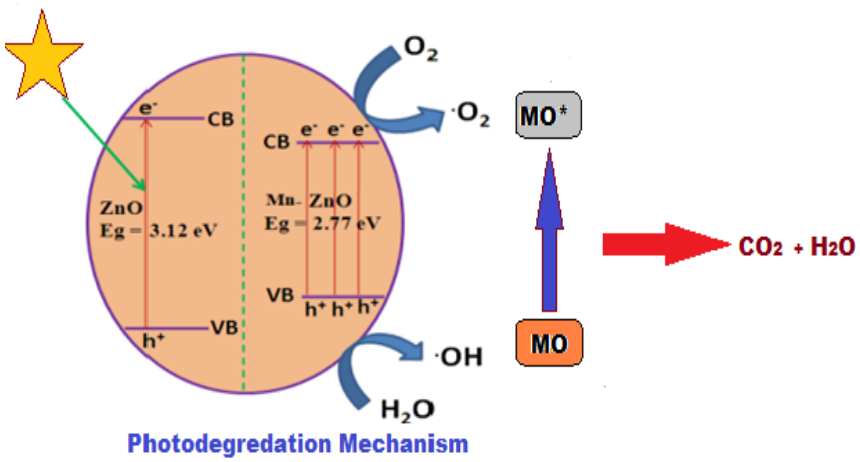

Graphical Abstract

Because ZnO absorbs weakly in the visible spectrum, it only possesses a small amount of photocatalytic activity on its own. In this study, a sol-gel technique is used to create manganese (Mn) doped zinc oxide (ZnO) nanoparticles with Mn concentrations varying from (0,2,4 wt%). ZnO nanoparticles with manganese doping had a larger visible light absorption band that extended from 400 nm to 700 nm. To further explain it, X-ray diffraction, FT-IR, FESEM, EDAX and HRTEM were used. The XRD data show that the nanoparticles were properly crystallised and had a hexagonal wurtzite structure while the EDAX results show that manganese was doped into the ZnO structure.

FESEM scans revealed the granular form of the nanoparticles without any flaws, supplying additional proof that manganese doping reduces grain size. The FT-IR signal denotes the formation of a connection between functional groups and metal oxide. High-resonance transmission electron microscopy studies show that both undoped and Mn-doped ZnO crystallites can form Wurtzite structures which have a mean size of 50–20 nm. This is in line with the crystallite size that Scherer's formula predicts[2,6,22].

The components of the un-doped and doped nanoparticles were identified via EDAX research. In comparison to undoped ZnO nanostructures, ZnO nanoparticles with manganese doping have shown enhanced photocatalytic activity for the degradation of the dye methyl orange. Manganese doping of ZnO nanoparticles promotes an improvement in photocatalytic activity by shrinking the grains and enhancing light absorption to include the visible spectrum[43].

Material and Methods

Materials: Only analytical-grade compounds, which were not further refined before use, were employed throughout this study. It used zinc acetate di-hydrate and manganese acetate as sources of zinc and manganese respectively. The same grade is used to buy sodium hydroxide, ethanol and methylene orange (molecular formula: $C_{14}H_{14}N_3NaO_3S$, molecular weight: 319.85 g/mol, max = 660 nm). All of the 99.5% pure chemicals used for the study were bought from Sigma-Aldrich, Mumbai, India. Every chemical tested positive for purity. After being completely cleaned in acid, all of the equipments were carefully rinsed with tap water and then with distilled water. Deionized water was used as the experiment's solvent throughout the entire process[1,7,30,36].

All other chemicals and reagents, including the 99.5% pure methylene red dye, were purchased from Sigma-Aldrich. Prior to usage, the entire glassware was carefully washed with distilled water and an acid wash. Each experiment was carried out with deionized (DI) water.

Collection of Dragon fruit peel: During post-monsoon (April 2023), dragon fruits were collected from local fruit shops.

Preparation of Dragon fruit peel extract: To eliminate the pulp, the dragon fruits' peels were split open. The pulp was freeze-dried using a Christ Freeze Dryer Alpha 1-4LD plus for 48 to 72 hours at -50 °C and 0.040 mbar. After using an MRC knife mill cup to grind the sample into a powder, it was stored at -80 °C until it was required.

Synthesis of Zirconium oxide nanoparticles using Dragon fruit peel extract: 10 ml of fruit extract received individual applications of 0.1M, 0.3M and 0.5M zinc oxide solutions before being agitated for three hours at 80°C. Then, to further purify it, it was centrifuged for 30 minutes at 5000 rpm. After that, it was periodically rinsed with deionized water. After that, it was maintained for two hours at 120°C in a hot air oven. Calcination at 500°C for four hours resulted in the creation of the dark brown powder. The same procedure was being employed for the 0.3M and 0.5M preparations respectively.

The synthesis of Mn-ZnO NPs was confirmed by the light-to-dark brown transition of the reaction mixture. The conversion of Zn^{2+} ions to Zn by phenolic compounds, which are abundant in CFE, provides an explanation for this. Fruit extracts have been found to operate as a reducing agent as well as a capping agent for the metal nanoparticles[21,44].

Dragon Fruits and peel collections

Synthesis of Manganese doped zinc oxide nanoparticles: The starting solution was made by combining 0.1 M solution of zinc acetate di-hydrate $Zn(CH_3Coo)_2.2H_2O$ with ethyl alcohol. The right quantity of manganese acetate $Mn(CH_3Coo)_2•4H_2O$ in 0, 2 and 4 wt% deionized water was added to the aforementioned solution. The supplementary solution included 20 mM NaOH and 10 mL of ethanol. The initial temperature for these three solutions was 50 °C. Zinc acetate solution was heated in the round bottom flask before manganese acetate solution was added. 80°C was reached while continuously stirring the zinc and manganese acetate solution for 30 minutes. Refluxing $Zn(CH_3Coo)_2.2H_2O$ and $Mn(CH_3Coo)_2•4H_2O$ into a solution was the next step, to which NaOH solution was then added drop by drop.

The solutions were heated to 60-70°C once more and magnetically stirred for two hours. The solution was then cooled to room temperature. After the precipitate had formed, it was repeatedly washed with distilled water before receiving an ethanol treatment. The precipitate needed to be washed with ethanol to remove the unwanted salt and impurities. The finished item was kept at 550°C for 5 hours in a Muffle furnace. In the absence of a manganese source, the similar procedures were used to produce pure ZnO nano particles[4,20,27,28].

Photocatalytic Experiments: To test a synthetic photocatalysts performance in determining the pollutant's photocatalytic discolouration efficiency, 30 ppm of the contaminant model methyl orange was combined with UV light. A UV light source (WSFSWL ultraviolet lamp with specified voltage 220 V, nominal wattage 30 W) was used to efficiently destroy the dye in order to evaluate the efficacy of un-doped and Mn-doped nanoparticles. Un-doped and doped (0.2, 0.4M) ZnO nanoparticles were dissolved in 50.0 ml of a 10 mg/L MO dye solution. The mixture was stirred in the dark for 30 minutes to allow the MO dye molecules to adhere to the Zn1-xMnxO nanoparticles' surface.

The homogeneous mixture (200 W) was exposed to Xenon lamp illumination. Five millilitres of the aqueous dispersion were sampled after being subjected to radiation for ten minutes and the nanomaterial was separated using centrifugation. The amount of MO that was still present in the supernatant liquid, was measured using a UV spectrophotometer. The following formula was used to determine the photo catalytic efficiency[3,13,41].

% of decoloration of color = $(1 - C/C_0)$.

where the MO dye solution's initial concentration is C_0 and the residual MO dye solution concentration is C.

Characterization: In the scan range of 20°C to 80°C at room temperature, a Philips PW 137 X-ray diffractometer (XRD) with a Cu source (k=1.5406) was used to measure the crystalline character of the produced products. Both HRTEM (TEM-2100 plus electron microscope) and EDAX (AZTEC/Xact) were used to confirm the findings of the morphological and compositional analyses of components conducted by the FESEM (HITACHI SO-6600, Japan). Utilising UV-Vis spectroscopy, the CARY 5E UV-Vis spectrometer was used to investigate optical properties in the 200-800 nm wavelength range. The functional groups of the substances were estimated by a 5DX FTIR spectrometer. The chemical states of the elements contained in the nanoparticles were determined using X-ray photoelectron spectroscopy (XPS)[24,32,42].

Results and Discussion

Analysis of X-ray diffraction: Fig. 1 shows the XRD patterns of Mn-doped and un-doped ZnO NPs. The structural properties of pure and Mn-doped ZnO nanoparticles have been studied using XRD in the 2 range, which spans between 0 and 800. The (100), (002), (101), (102), (103), (112) and (203) planes of the miller indices correspond to the 2 values 31.950, 34.610, 36.430, 47.730, 56.780, 63.050, 68.130 and 69.260 respectively. Each of the diffraction peaks' underlying hexagonal wurtzite structures is in agreement with JCPDS card no. 36-1451. The impurity peaking does not exist in the doped samples. The diffraction peaks of doped samples are slightly different from those of pure ZnO by shifting lower, as seen in figure 1. This could be due to Mn^{2+} substitutions at Zn^{2+} sites in the ZnO lattice.

Scherer's formula can be used to determine the typical crystallite size. In contrast to the samples that contain Mn doping, which have smaller crystallite sizes, pure ZnO is measured to have an average crystalline size of 49.5 nm. It has been found that the average crystallite size tends to decrease as Mn concentrations increase[5,25,31].

FT-IR Spectroscopy: The KBr pellet method is used to capture solid phase FT-IR spectra in the 4000-400cm^{-1} region. Each sample's FT-IR spectrum is shown in figure 2. Figure 2 shows clear variations in the locations and sizes of the IR peaks, suggesting that Mn may have been absorbed into the ZnO host. The band at 632 cm^{-1} could be explained by the anti-symmetric Zn-O-Zn stretching mode whereas the band between 480 and 510 cm^{-1} is caused by symmetric Zn-O-Zn and Mn-O bonds. The peak that occurs at 1120 cm^{-1} is connected to the vibration of the hydroxyl-tin (Zn-OH) bond. The vibration at 1340 cm^{-1} is caused by the C-O stretching mode connected to the citrate complex. Since the carboxylic groups are released in solid citrate, the vibration of C=O stretching is thought to be the cause of the peak at 1602 cm-1. The strong bands between 3430 and 1602 cm^{-1} demonstrate the presence of absorbed water.

Strong agreement exists between the values given in the pertinent literature and the actual allocations[15,17,33,44]. The diagonal optical mode must swing downward in this investigation's of Mn ion replacement and the peak must transfer to the doped sample's vibrational modes, which must be acceptable at frequencies of 480 cm^{-1} and higher.

UV–Visible spectroscopic study: UV-visible spectroscopy was used to examine the optical properties of un-doped and Mn-doped ZnO nanoparticles. The optical measurements were performed by UV-Vis diffusion reflectance spectroscopy to confirm the substitution of Zn^{2+} for Mn^{2+}. Figure 3 shows the spectra of samples of pure and Mn-doped ZnO for UV-Vis diffusion reflectance. Due to the relatively high stimulating binding energy, it has been discovered that the absorption edge between 300 and 370 nm and the higher Mn concentration both decrease the optical transparency of pure ZnO.

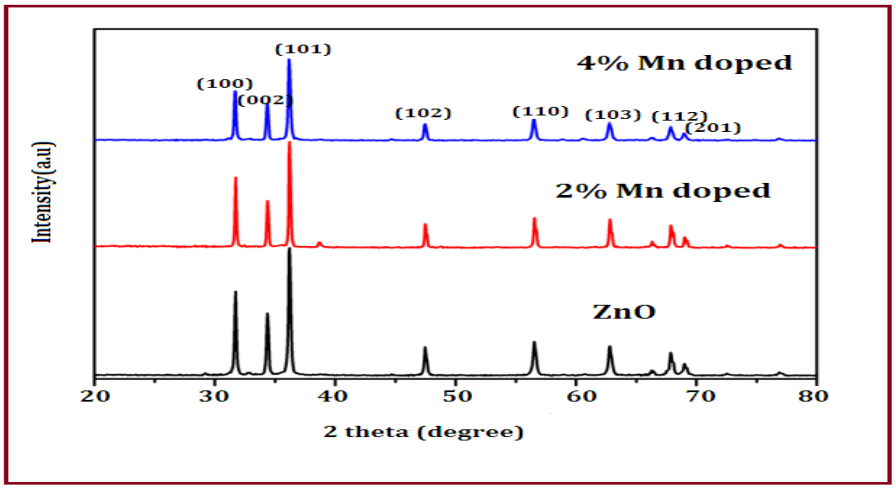

Fig. 1: XRD array of Un-doped, 0.2M Mn/ZnO and 0.4M Mn/ZnO nanoparticles

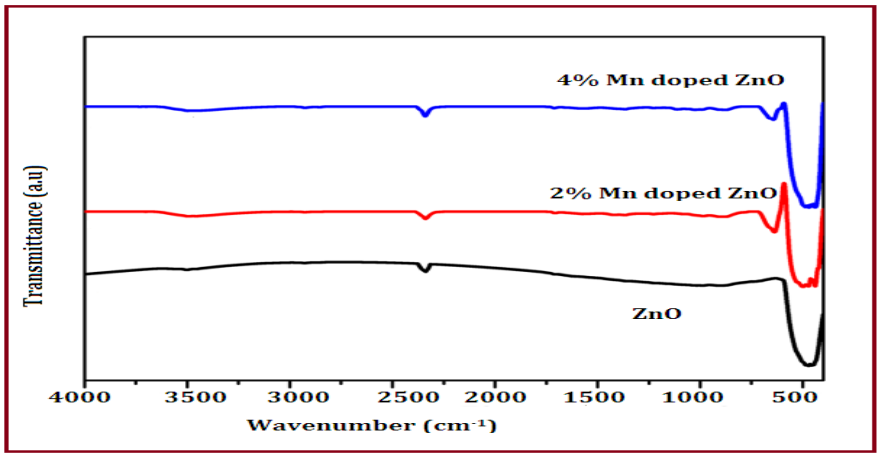

Fig. 2: FT-IR spectrum of Un-doped, 0.2M Mn/ZnO and 0.4M Mn/ZnO nanoparticles

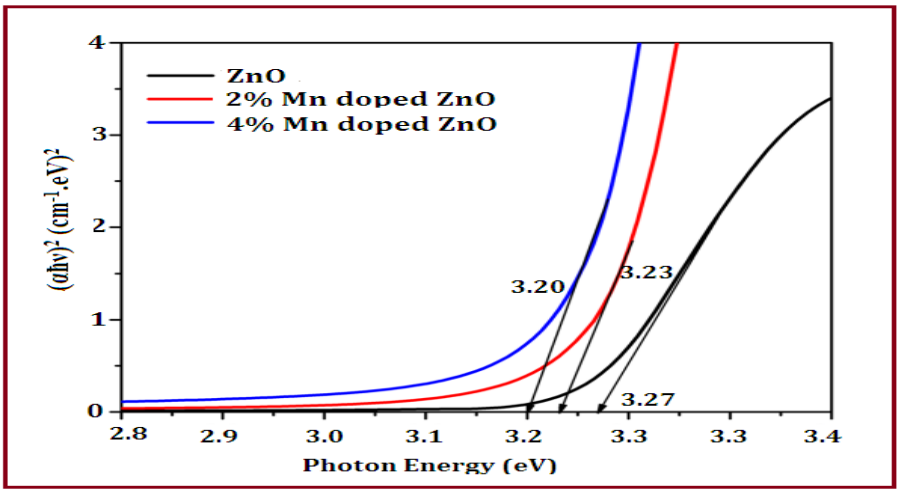

Fig. 3: UV-DRS spectrum Undoped, 0.2M Mn/ZnO and 0.4M Mn/ZnO nanoparticles

The absorption margins significantly redden as Mn concentration rises from 0 to 4 wt %; this indicates that doping has narrowed the band gap of ZnO. Band gap energy was assessed using the K-M model[8,11]. The optical band gap of Mn doped ZnO decreases from 3.27 eV to 3.20 eV as Mn content (0–4% wt %) is raised. The development of an incorrect energy level in the ZnO optical band gap between the valence and conduction bands is most likely the root of the Mn doped ZnO's absorption wavelength range red shift.

This may be due to the incorporation of Mn^{2+} into the ZnO lattice, which led to a significant sp-d energy exchange between the s and p electrons in the ZnO conduction band and the d electrons of Mn. This allowed the conduction band to move downward and decreased the energy of the forbidden band. As shown by the lowered band gap value of the final dopant Mn on ZnO semiconductors in this work, an effective nano photo catalyst has been produced[29,40].

FESEM-EDAX analysis: The surface morphology and energy dispersive scattering (EDAX) pattern of nanoparticles of Mn-doped and un-doped ZnO are analysed using FESEM. Researchers can analyse the morphological and compositional actions of solid sample surfaces using a high resolution microscope. Huge aggregates of uniform nanoparticles can be seen in fig. 4 and the doped samples are more accumulated than the pure ZnO samples. The typical size of pure ZnO is found to be about 50 nm, however as manganese doping concentration increases, the average size decreases, as demonstrated in the XRD data[35].

Mn-doped ZnO nanoparticles are crystalline and have elongated spherical flakes as their structure, un-doped ZnO is crystalline and has a spherical structure. EDAX spectra were also utilized to confirm the elemental makeup of the created nano-photocatalyst. Figure 4d shows the Mn-doped and un-doped ZnO nanoparticles' EDAX spectra. The presence of zinc, manganese and oxygen atoms in the synthesised nanoparticles may be seen by the emission of continuous, high-pitched peaks with zinc oxide and manganese-zinc oxide (Zn: 52.49% O: 44.77% Mn: 2.74%). Over the entire scanning range, there were no visible impurity peaks[8,38].

HRTEM analysis: A HRTEM picture with SAED inserts was shown in fig. 5. Pure ZnO nanoparticles have a cubic spherical form and a typical size of about 20 nm, but they aggregate because the grain boundary is not clearly defined. When doping concentrations are higher than 0.2 or 0.4M, the grain size changes and the image seems to be comprised of spherical flakes about 12 nm in width. While possessing diffuse grain and grain border properties, Mn-doped ZnO nanoparticles have a dense nanostructure that is particularly beneficial in boosting their photocatalytic activity.

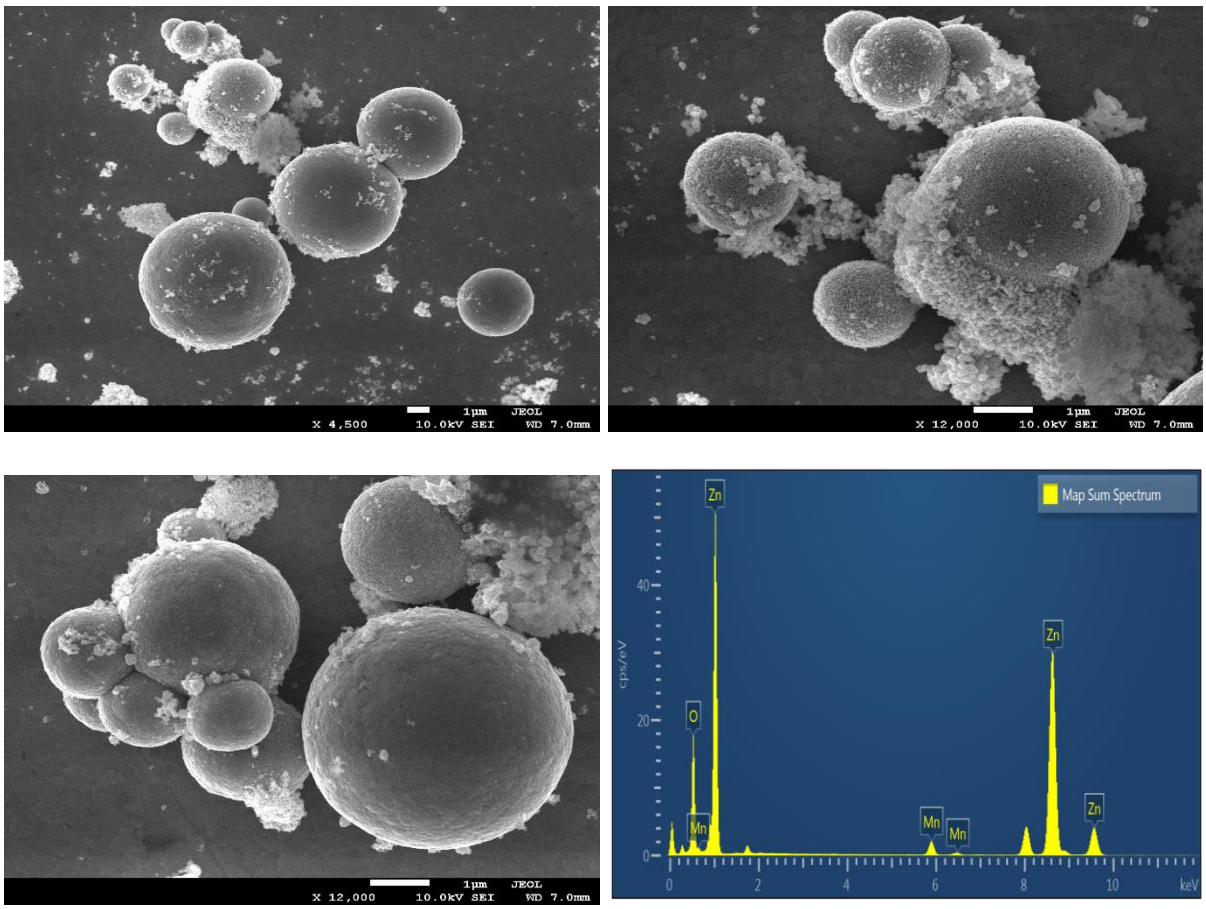

Fig. 4: FESEM images of (a) Undoped ZnO (b, c) 0.2M Mn/ZnO,0.4M Mn/ZnO (d) EDAX spectrum of Mn doped ZnO nanoparticles

The insets of each figure demonstrate how the ZnO nanostructure's d-spacing fits the SAED rings' ability to reflect light. The images show a typical lattice spacing that corresponds to the (001) and (101) planes of the ZnO crystal. Starting from the SAED pattern, the ZnO and Mn-doped ZnO nanocrystals have arbitrary orientations[14,37,39].

Photocatalytic activity measurements: Utilising the breakdown of methyl orange dye, the photocatalytic activity of un-doped and Mn-doped ZnO nanoparticles was assessed. The results showed that the quantity of photocatalysts and exposure time had a significant impact on how quickly reactive dyes degrade.

The variation in degradation effectiveness with radiation exposure time is seen in figure 6. After UV exposure, the percentage of MO dye concentration that declines in the presence of typical pure and Mn (2 and 4 wt %) doped ZnO materials has been graphed in fig. 6.

Higher Mn ion concentrations increased the Mn-doped ZnO samples' photocatalytic activity. With a reaction period of 120 minutes, the methyl orange degradation efficiencies of Mn doped (2 and 4 wt.%) ZnO samples are approximately 36, 45 and 78% respectively. After 120 minutes of UV light irradiation, the photocatalytic activity of methyl orange was tripled when Mn (4 wt%)-doped ZnO samples were used. By significantly boosting the photocatalytic activity (78%), Mn^{2+} doping demonstrated the maximal photocatalytic performance of MO decolonization.

The same photocatalysts are gathered and utilised repeatedly. The potential for reuse of samples of Mn (4 wt%)-doped ZnO is also investigated. The photocatalytic activity of the Mn-ZnO samples shows some degeneration after seven cycles of photo methyl orange degradation, as seen in fig. 7, due to insufficient memory and loss during washing. Mn-ZnO samples used as photocatalysts are an excellent option due to their stability and significant potential for application in water treatment.

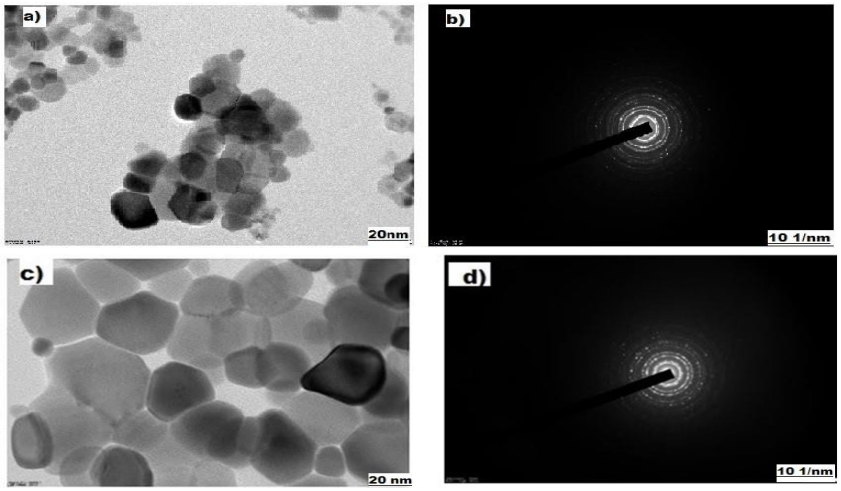

Fig. 5: HRTEM images of (a) 0.2M Mn/ZnO (c) 0.4M Mn/ZnO (b,d)SAED pattern of Mn doped ZnO

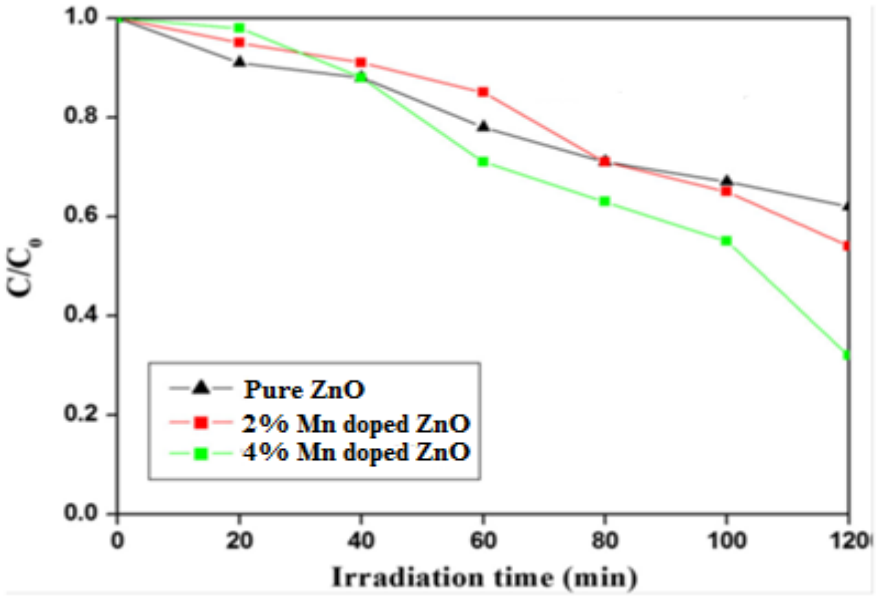

Fig. 6: Photo catalytic degradation % of Methyl Orange by un-doped ZnO and Mn doped ZnO

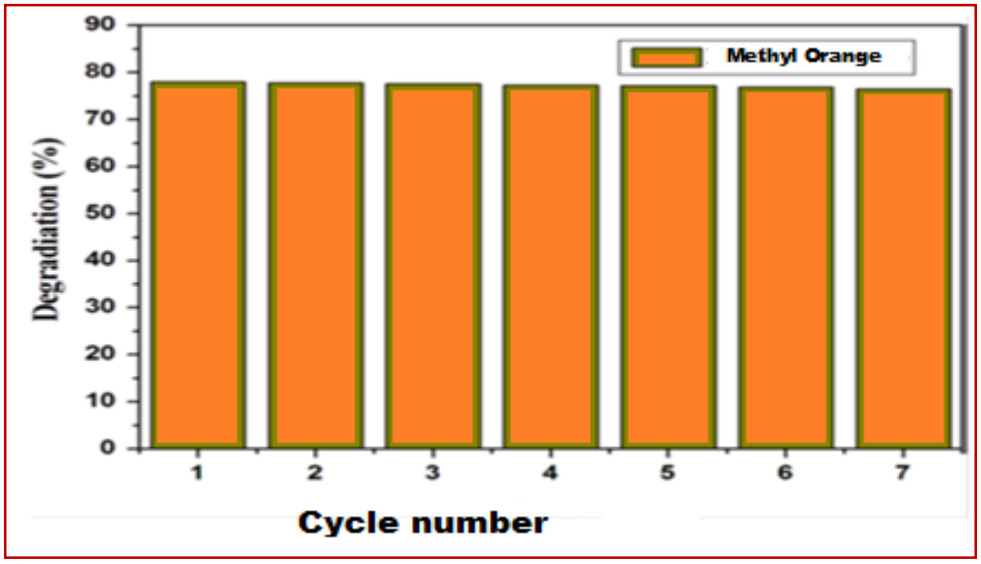

Fig. 7: Reusability Test of Mn doped SnO_2

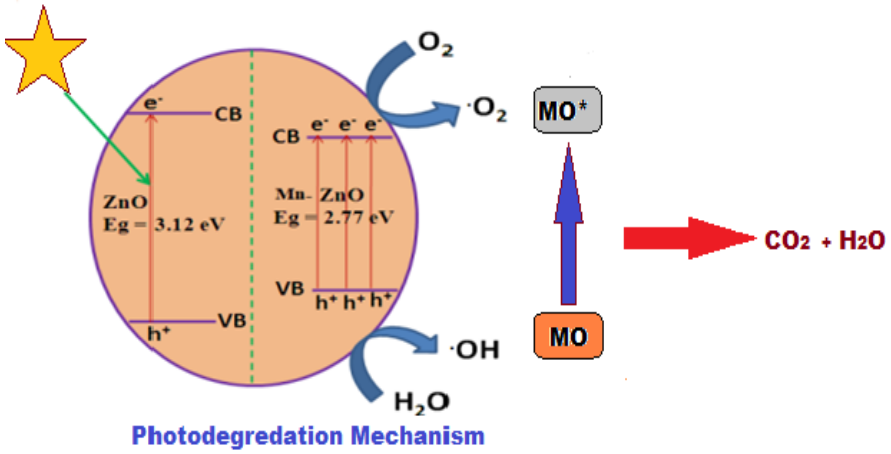

Fig. 8: Mechanism of Photocatalytic degradation

The photocatalytic activities of the catalyst are strongly influenced by its shape, size, band gap energy and surface modification. Mn doping could be used to achieve these. Given the smaller particle size and higher band gap energy of ZnO, the increased photocatalytic activity of Mn-doped samples may be attributed to the emergence of accepting energy levels below the conduction band. The photocatalytic mechanism of MO by Mn-doped ZnO catalysts is shown in fig. 8. Although ZnO with a band gap energy of 3.12 eV in the current experimental setting theoretically activated by photons with wavelengths below 363 nm only displays a tiny level of photocatalytic activity.

The quick recombination of the photogenerated electron-hole pairs in ZnO is the most likely culprit for this. Mn-doped ZnO, which has a band gap energy of 3.20 eV which may be excited by photons with wavelengths less than 384 nm. ZnO has a lower CB when compared to ZnO with Mn doping. The photogenerated electrons can so travel back in time[10,26]. The Mn-doped ZnO nanoparticles may contain photogenerated holes which would increase the efficiency of charge separation and hence boost the photocatalytic activity of the Mn-doped catalyst[11,16,34]. Electrons may only go in one direction, whereas holes can move in either direction.

The photo-excited electron's transition to the conduction band is improved as more MO molecules are adsorbed on the surface of the Mn-ZnO catalyst and at the same time, the amount of electron transport to the adsorbed O_2 rises. The reduced band gap energy of the Mn doped ZnO may also play a significant role in increasing the visible light photocatalytic activity of ZnO catalyst.

Conclusion

Finally, using the sol-gel method, we successfully created pure and Mn doped ZnO nanoparticles. ZnO has a hexagonal wurtzite type crystal structure, according to powder XRD tests and the results are in good agreement with the required JCPDS data (card no. 36-1451). FESEM identified an expanded spherical form with an average particle size of 50 nm. It was feasible to observe a large red shift and a drop in the band gap energy from 3.12 to 2.77 eV by looking at UV-Vis spectra. Additionally, Mn-doped ZnO had photo absorption that reached beyond the visible light spectrum,

according to UV tests. It was claimed that the presence of Mn dopant caused the concentration of impurities in ZnO's conduction and valence bands to rise, resulting in a narrower band gap and more visible light absorption.

By exposing MO to the visible spectrum, the photocatalytic effectiveness of pure and Mn-doped ZnO catalysts was assessed. When compared to un-doped ZnO, Mn-doped catalysts have the best photocatalytic activity. The recycling test demonstrates that the degradation rate of the Mn-ZnO catalyst is almost consistent and that there was no activity loss over the first four cycles. The result suggests that Mn-doped ZnO catalyst may have significant applications in the treatment of waste water as well as the elimination of pollution as particularly efficient photocatalysts.

Acknowledgement

To conduct the study, we are grateful for the lab facilities offered by Panimalar Engineering College, Chennai-600123, India.

References

1. Alshgari Razan A., Harishchander A., Kistan A., Nisha N., Vel V M., Anitha G., Saikh Mohammad W., Islam M.A. and Agonafir A., Experimental Investigations on the Mechanical Characteristics of Natural Fiber Particle-Reinforced Polymer Composites under Cryogenic Environment, *Journal of Nanomaterials*, **1**, 8 **(2022)**

2. Ashwini K., Shetty Vijith V., Raghotham Ananthan, Shetty Praveen Kumar and Suchetha Kumari N., Study on in vitro therapeutic impact of 17-β Estradiol on Glioblastoma cell lines, *Res. J. Biotech*., **18(12)**, 1-6 **(2023)**

3. Bachmann S.A.L., Nunes K.G.P., Calvete T. and Féris L.A., Low-cost adsorbents prepared from brewers spent grain for pollutants removal, *Emergent Materials*, **6(2)**, 741-753 **(2023)**

4. Bailey S.E., Olin T.J., Bricka R.M. and Adrian D.D., A review of potentially low-cost sorbents for heavy metals, *Water Research*, **33(11)**, 2469-2479 **(1999)**

5. Chawla S. and Jayanthi S.K., Fabrication of ZnO: Mn nanoparticles with organic shell in a highly alkaline aqueous environment, *Appl. Surf. Sci*., **257**, 2935–2939 **(2011)**

6. Chitra M., Kistan A., Kanchana V. and Jayanthi A., Sol-Gel synthesis, characterization and photocatalytic activity of Cobalt doped ZnO nanoparticles, *Res. J. Chem. Environ*, **28(3)**, 48-55 **(2024)**

7. Dabin Y. and Wang D., Synthesis of ITO nanowires and nanorods with corundum structure by a co-precipitation-anneal method, *Mater. Letters*, **58**, 84–87 **(2006)**

8. Du M., Orava A., Prodan G. and Moscalu F., Investigations on the influence of surfactant in morphology and optical properties of zinc oxide Nano powders for dye-sensitized solar cells applications, *Mater. Sci. Semicond. Process*, **16**, 1095**(2013)**

9. Elimelech M. and Phillip W.A., The future of sea water desalination: energy, technology and the environment, *Science*, **80**, 712–717 **(2011)**

10. Gayathri R., Raja G. and Rajeswaran P., A simple and one step low cost microwave induced low cost Graphene modified CeO_2 photoelectrodes for high efficiency dye-sensitized solar cells, *Inorganic Chemistry Communications*, **120**, 08132 **(2020)**

11. Hariharan V., Parthibavarman M. and Sekar C., Synthesis of tungsten oxide ($W_{18}O_{49}$) nanosheets utilizing EDTA salt by microwave irradiation method, *J. Alloy. Compd*, **509**, 4788 **(2011)**

12. He R., Hocking R.K. and Tsuzuki T., Local structure and photocatalytic property of sol–gel synthesized ZnO doped with transition metal oxides, *J. Mater. Sci*, **47**, 3150-3158 **(2012)**

13. Huang Y., Wu C., Zhai M., Sun Y. and Liu Sens J., Fabrication and gas-sensing properties of hierarchically porous ZnO architectures, *Actuators B*, **155**, 126–133 **(2011)**

14. Kali A., Amar A., Loulidi I., Jabri M., Hadey C., Lgaz H. and Boukhlifi F., Characterization and adsorption capacity of four low-cost adsorbents based on coconut, almond, walnut and peanut shells for copper removal, *Biomass Conversion and Bio Refinery*, **14(3)**, 3655-66 **(2024)**

15. Kanchana V., Kistan A., Sakayasheela L., Sumathi J., Premkumar A. and Selvam A., Titanium dioxide as a Catalyst for Photodegradation of Various Concentrations of Methyl Orange and Methyl Red dyes using Hg Vapour Lamp with Constant pH, *Oriental Journal of Chemistry*, **34**, 2 **(2018)**

16. Kapil S., Sharma V. and Kumar T., Characterization of Bacillus tequilensis A1C1: A Novel Bio-reservoir of D-serine, *Res. J. Biotech*., **18(2)**, 8-14 **(2023)**

17. Kistan A. and Kanchana V., Silver-Alumina Impregnated Maghemite/Magnetite Nanocomposites for Effective Removal of Chromium (VI) from the Tannery Discharge, *Asian Journal of Chemistry*, **35**, 1899-1906 **(2023)**

18. Kistan A. and Kanchana V., Confiscation of chemical oxygen demand from groundwater samples collected from near tanneries using activated carbon of Ricinus Communis blended with coconut shell, *Indian Journal of Environmental Protection*, **40**, 527–532 **(2020)**

19. Korosi L., Papp S., Meynen V. and Dekany I., Preparation and characterization of SnO_2 nanoparticles of enhanced thermal stability: The effect of phosphoric acid treatment on $SnO_2 \cdot nH_2O$, *Colloids Surf A Physicochem Eng Asp*., **268**, 147–154 **(2005)**

20. Lee W.W., Chung W.H., Lu C.S., Lin W.Y. and Chen C.C., A study on the degradation efficiency and mechanisms of ethyl violet by HPLC and GCMS, *Sep. and Purify. Tech*, **98**, 488e96 **(2012)**

21. Liu Y., Zhao S., Qiu X., Meng Y., Wang H., Zhou S. and Yan C., Clinoptilolite based zeolite-geopolymer hybrid foams: potential application as low-cost sorbents for heavy metals, *Journal of Environmental Management*, **330**, 117167 **(2023)**

22. Liu Y., Han J., Qiu W. and Gao W., Hydrogen peroxide generation and photocatalytic degradation of estrone by microstructural controlled ZnO Nano rod arrays, *Appl. Surf. Sci*., **263**, 389 **(2012)**

23. Mohan S., Kistan A., Mahalakshmi S., Jayanthi A., Ramya A. and Karthik Siva P., Sol-Gel technique, characterization and

photocatalytic degradation activity of Manganese doped ZnO nanoparticles, *Main Group Chemistry*, **24**, 1-8 **(2023)**

24. Murugadoss G., Synthesis and Characterization of Transition Metals Doped ZnO Nanorods, *J. Mater. Sci. Technol*, **28**, 587–593 **(2012)**

25. Nisha Mary U., Venkatesh D., Arulmurugan S., Kistan A., Rajeshwaran P. and Siva Karthik P., Assessment of solar light sensitive Chitosan integrated CeO2-CuO ternary composites for the efficient degradation of Malachite Green, Acid Blue 113 dyes and microbial studies, *Inorganic Chemistry Communications*, **160**, 111942 **(2023)**

26. Pant H.R., Pant B., Sharma R.K., Amarjargal A., Kim H.J., Park C.H., Tijing L.D. and Kim C.S., Antibacterial and photocatalytic properties of Ag/TiO_2/ZnO nano-flowers prepared by facile one-pot hydrothermal process, *Ceram. Int*., **39**, 1503–1510 **(2013)**

27. Premkumar A., Kistan A. and Kanchana V., A Simple Treatment of Tannery Wastewater using Modified Activated Carbon by Metal Chloride, *Asian J. Chem*., **34**, 1698-1702 **(2022)**

28. Qiao M., Wei K., Ding J., Liu Z., Zhang K.Q. and Huang X., Decolorizing activity of malachite green and its mechanisms involved in dye biodegradation by A Chromobacter xylos oxidans MG1, *J Mol Microbiol Biotechnol*., **20**, 220e7 **(2011)**

29. Rajeswaran P., Shanmuga Sundari T. and Shanmuganathan M., A simple fabrication of Mn doped SnO_2 nanoparticles towards improved Congored degradation photocatalytic activity, Materials Today Proceedings, **2214,** 7853 **(2022)**

30. Santhosh C., Velmurugan G., Jacob S.K., Jeong A.N. and Grace A., Role of nanomaterials in water treatment applications: a review, *Chem. Eng. J*., **306**, 1116–1137 **(2016)**

31. Sakai G., Baik N.S., Miura N. and Yamazoe N., Gas sensing properties of tin oxide thin films fabricated from hydrothermally treated nanoparticles: Dependence of CO and H_2 response on film thickness, *Sens. Actuators B*., **77**, 116 **(2001)**

32. Sathiyamoorthi R. and Kistan A., Intensification of Bio-synthesis of Zirconium Oxide (ZrO_2) nanoparticles derived from novel Crescentia Cujete fruits: Effects on diesel engine characteristics powered by Waste Engine oil methyl ester-Diesel blend, *Chemical Engineering and Processing-Process Intensification*, **195**, 109642 **(2023)**

33. Sayılkan F., Asiltu M., Tatar P., Kiraz N., Arpac E. and Sayılkan H., Preparation of re-useable photocatalytic filter for degradation of Malachite Green dye under UV and visirradiation, *J. Hazard Mater.*, **44**, 148 **(2007)**

34. Singh P., Kumar R. and Sing R.K., Progress on transition metal-doped ZnO nanoparticles and its application, *Industrial & Engineering Chemistry Research*, **58**, 17130 **(2019)**

35. Sun L., Shao R., Chen Z., Tang L., Dai Y. and Ding J., Alkali-dependent synthesis of flower-like ZnO structures with enhanced photocatalytic activity via a facile hydrothermal method, *Appl. Surf. Sci*, **258**, 5455–5461 **(2012)**

36. Tennakone K. and Bandara J., Photocatalytic activity of dye-sensitized tin (IV) oxide monocrystalline particles attached to zinc oxide particles: long distance electron transfer via ballistic transport of electrons across Nano crystallites, *Appl. Catal. Part A. Gen*, **208**, 335 **(2001)**

37. Topare N.S. and Wadgaonkar V.S., A review on application of low-cost adsorbents for heavy metals removal from wastewater, Materials Today: Proceedings, **77**, 8-18 **(2023)**

38. Vijaya Anandan V.A., Kistan A., Saral A. and Thaminum Ansari A., Retarding of Preliminary Chemical Pollutants from Dye Effluent by Metal Nano Particles Synthesized using Flower Extract of Catharanthus Roseus, *Oriental Journal of Chemistry*, **34**, 381 **(2018)**

39. Viswanatha R., Sapra, S., Gupta S., Satpati B. and Satyam P.V., Synthesis and characterization of Mn-doped ZnO nanocrystals, *Phys. Chem. B.*, **108**, 6303–6310 **(2004)**

40. Weng B., Qi M.Y., Han C., Tang Z.R. and Xu Y.J., Photo corrosion inhibition of semiconductor-based photocatalysts: basic principle, current development and future perspective, *ACS Catalysis*, **9**, 4642 **(2019)**

41. Xie W., Li Y., Sun W., Huang J., Xie H. and Zhao X., Surface modification of ZnO with Ag improves its photocatalytic efficiency and photostability, *J. Photochem. Photobiol. A*, **216**, 149–155 **(2010)**

42. Yang M. and Guo Z.X., Synthesis and characterization of Mn-doped ZnO column arrays, *Appl. Surf. Sci.*, **256**, 4201 **(2010)**

43. Zhaohui H., Neng G., Wanqun Z., Huaquiao Z. and Yitai O., Solvothermal preparation and morphological evolution of stannous oxide powders, *Mater. Letters*, **48**, 99–103 **(2001)**

44. Zhang Y.R., Wan J and Ke Y.U., A novel approach of preparing TiO_2 films at low temperature and its application in photocatalytic degradation of methyl orange, *J. Hazard Mater*., **177**, 750–754 **(2010)**.

(Received 14th February 2024, revised 01st December 2024 accepted 06th December 2024)